JOURNAL OF COMPUTATIONAL PHYSICS 120, 88–104 (1995)

A Vortex Sheet Method Applied to Unsteady Flow Separation from Sharp Edges

M. C. A. M. PETERS* AND H. W. M. HOEIJMAKERS

Eindhoven University of Technology, W & S 1.46, P.O. Box 513, 5600 MB Eindhoven, The Netherlands

Received February 16, 1994; revised December 30, 1994

A computational method is presented which describes the unsteady two-dimensional vortex generation and convection in stationary geometries with sharp edges. A second-order panel method is used to describe the motion of the two-dimensional vortex sheet, while the generation of vorticity at the sharp edges is enforced through a Kutta condition. In order to easily satisfy the normal-velocity boundary condition on the stationary walls, the flow domain is transformed to a half-plane ($x > 0$) by a Schwarz–Christoffel conformal mapping. In the computational plane the solid walls are situated on the vertical coordinate axis so that image vorticity can be utilized to satisfy the boundary condition in a simple way. The method is applied to describe the separating impulsively started flow past a sharp-edged wedge and the flow in a channel with a deep cavity. These applications show that the method is able to describe vortex shedding in complex geometries in an accurate way.

1. INTRODUCTION

The problem of the generation and convection of free shear layers has been studied since the beginning of this century. For high Reynolds numbers, free shear layers can be modeled by infinitesimally thin vortex sheets, representing the vorticity, and a potential flow elsewhere. The study of the Kelvin–Helmholtz instability of a straight vortex sheet of uniform strength by Rosenhead [1] was the first attempt to describe the motion of a vortex layer numerically, employing a method in which the continuous vortex sheet is represented by a number of discrete vortices. Other flow problems where discrete vortex models have been used are the rolling-up of the vortex sheet behind an elliptically loaded wing, a delta wing, or a ring wing. Although a discrete vortex approach is not a very accurate description of a continuous vortex sheet, the model is still widely used in the literature because of its simplicity.

One of the problems of the point vortex method is that for a starting flow the method is not stable in the limit of the number of vortices going to infinity. The velocity induced by a point vortex of fixed circulation representing a portion of the vortex sheet tends to infinity when the distance to the vortex goes to zero and as a result the motion of a number of point vortices in close proximity inevitably leads to chaotic motion [2]. A number of methods have been proposed to solve this problem. The vortex blob method [3, 4] has proven to be most successful. In the vortex blob method the vorticity is not limited to a single point, but distributed in a small area around the centre of vorticity of the vortex blob. A densely packed row of these vortex blobs therefore describes a vortex layer of finite thickness. As a result the assumption of potential flow in the region outside the vortex sheet is lost in the region of the vortex layer. A number of reviews of the various discrete vortex methods used to describe the two-dimensional motion of vortex sheets can be found in the literature [5–10].

An alternative method to describe the vortex sheet more accurately has been proposed by Mokry and Rainbird [11]. In this method, the vortex sheet is described by a number of straight segments (so-called panels), with a panelwise uniform vortex distribution leading to a first-order accurate discretisation. Hoeijmakers and Vaatstra [12] developed a second-order accurate panel method in which the vortex sheet is described by a number of curved panels, carrying a piecewise linear vortex distribution. The method has been applied with success to describe the evolution of the free vortex sheet behind an elliptically loaded wing, the flow behind a ring wing, and a delta wing [12, 13].

These methods describe the motion of a vortex sheet after it has been generated and, furthermore, assume the absence of solid surfaces, which implies that the total vorticity contained in the vortex system is constant. In the present study the objective is to develop a method in which the walls and the generation of vorticity at sharp edges is incorporated so that the circulation can vary with time. Generation of vorticity has been achieved by imposing a so-called Kutta condition at the sharp edge. The implementation of the normal-velocity boundary condition at the solid walls has been accomplished employing a conformal mapping of the flow domain to a half-plane in which the solid wall is mapped onto an infinite straight wall and mirror-imaging can be applied to satisfy the boundary condition.

In Section 2 the computational method will be described,

* Present address: Shell Research B.V., Volmerlaan 6, 2288 GD Rijswijk, The Netherlands.

0021-9991/95 $12.00

where the application of the conformal mapping technique and the Kutta condition will be highlighted. In Section 3 two examples of the application of the method will be presented, the self-similar starting flow past an infinite wedge and the starting flow in a channel with a sharp-edged T-junction. The results will be compared with results of flow visualisation of the starting flow in a T-junction.

2. DESCRIPTION OF THE METHOD

2.1. Vortex Sheet Method

A detailed description of the second-order panel method describing the motion of the vortex sheet is given by Hoeijmakers and Vaatstra [12, 13]. In the vortex-sheet method the sheet is divided into a number of continuous segments (so-called *panels*), and the velocity field induced by the vortex sheet is evaluated as the sum of the contribution of all panels. The contribution of each panel to the velocity field is computed to a desired order of approximation. If the coordinates of the points on the vortex sheet are given by $z(s) = x(s) + iy(s)$, where s is the arc length parameter along the vortex sheet and the vortex distribution on the vortex sheet is given by $\gamma(s)$, then $z(s)$ and $\gamma(s)$ are described by piecewise polynomial representations, where the accuracy of the method is determined by the specific combinations of the degree of the polynomial chosen for $z(s)$ and $\gamma(s)$. The method is an extension of the first-order panel method, in which the panels are straight segments, with a panel-wise constant vortex distribution [11]. In the present second-order method the segments are curved and carry a linearly varying vortex distribution. In complex notation, the velocity $v = u_x + iu_y$ induced at a point z_0 by a vortex sheet is given by

$$v^*(z_0) = \frac{1}{2\pi i}\int_{s_0}^{s_\infty} \frac{1}{z_0 - z(s)}\, d\Gamma(s), \tag{1}$$

where a star denotes a complex conjugate, $\Gamma(s)$ is the dipole strength (local circulation) of the vortex sheet which is related to the vortex distribution through $d\Gamma/ds = -\gamma(s)$, and s_0 and s_∞ are the first and last points of the sheet, respectively. For a point z_0 close to the point $z(s_0)$ on the sheet, the velocity is given by

$$v^*(z(s_0)^\pm) = \mp\frac{1}{2}\gamma(s_0)\frac{dz^*}{ds}(s_0) + \frac{1}{2\pi i}\oint_{s_0}^{s_\infty} \frac{1}{z(s_0) - z(s)}\, d\Gamma(s), \tag{2}$$

where the integral $\oint$ denotes the Cauchy principal value of the integral and $\pm$ denotes the left- and right-hand sides of the sheet when moving along the curve in the direction of increasing arc length, respectively. Furthermore $dz(s)/ds$ is the unit tangential vector along the sheet. The jump of tangential velocity across the sheet is

$$v(z(s_0)^-) - v(z(s_0)^+) = \gamma(s_0)\frac{dz}{ds}(s_0); \tag{3}$$

the normal component of the velocity is continuous across the vortex sheet. On each panel, the dipole distribution and the geometry are expressed as

$$\Gamma(s) = \Gamma(s_j^*) + (s - s_j^*)\frac{d\Gamma}{ds}(s_j^*) + \frac{1}{2}(s - s_j^*)^2\frac{d^2\Gamma}{ds^2}(s_j^*) + \mathbb{O}(\Delta s_j^3) \tag{4}$$

$$z(s) = z(s_j^*) + (s - s_j^*)\frac{dz}{ds}(s_j^*) + \frac{1}{2}(s - s_j^*)^2\frac{d^2z}{ds^2}(s_j^*) + \mathbb{O}(\Delta s_j^3), \tag{5}$$

where s_j^* is the expansion point, chosen to be the midpoint of the panel and $\Delta s_j = s_{j+1} - s_j$ is the panel size in terms of the arc length. The velocity is to be calculated everywhere in the flow field, including at points situated on the vortex sheet. For the latter care must be taken to properly handle the singular character of the integrand in Eq. (2). Therefore a small curvature expansion of the integrand is used, in which $R(s) = z_0 - z(s)$ is approximated by the distance to the tangent of the panel at the expansion point plus a second-order term (see Fig. 1),

$$R(s) = R_f(s) - \tfrac{1}{2}(s - s_j^*)^2\frac{d^2z}{ds^2}(s_j^*) + \mathbb{O}(\Delta s_j^3) \tag{6}$$

with

$$R_f(s) = z_0 - z(s_j^*) - (s - s_j^*)\frac{dz}{ds}(s_j^*).$$

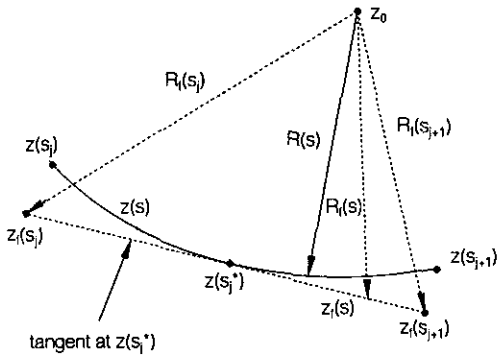

FIG. 1. The small curvature expansion used in the second-order panel method.

Substitution of this approximation into Eq. (1) gives the induced velocity in a second-order accurate approximation,

$$v_j^*(z_0) = \sum_{j=1}^{NP} \left[\frac{d\Gamma}{ds}(s_j^*) \left(E_0^j + \frac{d^2z}{ds^2}(s_j^*) E_1^j \right) + \frac{d^2\Gamma}{ds^2}(s_j^*) E_2^j \right] + \mathcal{O}(\delta_0^2), \tag{7}$$

where δ_0 is a measure of the average size of the panels on the sheet and the sum is taken over all panels NP. The second derivative of the coordinate $z(s)$ is related to the curvature $k_n(s)$ of the sheet according to $d^2z(s)/ds^2 = ik_n(s)\, dz(s)/ds$, since the curvature is defined as

$$k_n(s) = \Im\left[\frac{dz^*(s)}{ds} \frac{d^2z(s)}{ds^2} \right],$$

where $\Im(\ )$ denotes the imaginary part. Furthermore E_0^j, E_1^j, and E_2^j are given by

$$E_0^j = \frac{1}{2\pi i} \int_{s_j}^{s_{j+1}} \frac{1}{R_f(s)}\, ds$$

$$E_1^j = \frac{1}{2\pi i} \int_{s_j}^{s_{j+1}} \frac{\frac{1}{2}(s - s_j^*)^2}{R_f^2(s)}\, ds \tag{8}$$

$$E_2^j = \frac{1}{2\pi i} \int_{s_j}^{s_{j+1}} \frac{(s - s_j^*)}{R_f(s)}\, ds.$$

The integrands in Eqs. (8) can be expressed in closed form in a similar fashion as given by Hoeijmakers [13], i.e.,

$$E_0^j = \frac{-1}{2\pi i (dz/ds)(s_j^*)} \ln\left(\frac{R_f(s_{j+1})}{R_f(s_j)} \right)$$

$$E_1^j = \frac{1}{4\pi i (dz/ds)(s_j^*)} \left[\Delta s_j + \frac{2(z_0 - z(s_j^*))}{(dz/ds)(s_j^*)} \ln\left(\frac{R_f(s_{j+1})}{R_f(s_j)} \right) + \frac{(z_0 - z(s_j^*))^2}{(dz/ds)(s_j^*)} \left(\frac{1}{R_f(s_{j+1})} - \frac{1}{R_f(s_j)} \right) \right] \tag{9}$$

$$E_2^j = \frac{-1}{2\pi i (dz/ds)(s_j^*)} \left[\Delta s_j + \frac{z_0 - z(s_j^*)}{(dz/ds)(s_j^*)} \ln\left(\frac{R_f(s_{j+1})}{R_f(s_j)} \right) \right],$$

with $R_f(s_{j+1}) = z_0 - z(s_j^*) - \frac{1}{2}\Delta s_j (dz/ds)(s_j^*)$ and $R_f(s_j) = z_0 - z(s_j^*) + \frac{1}{2}\Delta s_j (dz/ds)(s_j^*)$.

The velocity induced at a point on the vortex sheet is mainly due to the velocity induced by the panel on which the point is situated. The velocity induced by a panel at its own midpoint can be derived from Eqs. (7)–(9) as

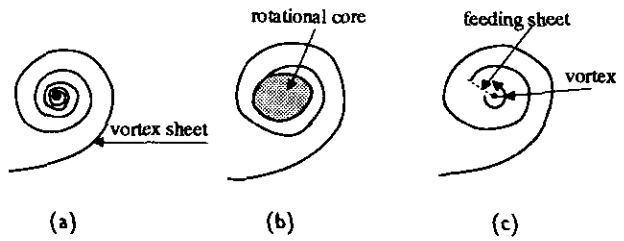

FIG. 2. Different core representations used to describe a strongly rolled-up vortex sheet: (a) rolled-up vortex sheet for Re $\rightarrow \infty$; (b) finite core method; (c) point vortex/feeding sheet method.

$$v_j^*(z(s_j^*)) = \left[-\tfrac{1}{2} \frac{d\Gamma}{ds}(s_j^*)\, \mathrm{sign}\,(\zeta) + \frac{1}{4\pi} \Delta s_j \frac{d\Gamma}{ds}(s_j^*) k_n(s_j^*) - \frac{\Delta s_j}{2\pi i} \frac{d^2\Gamma}{ds^2}(s_j^*) \right] \frac{dz^*}{ds}(s_j^*), \tag{10}$$

where $\mathrm{sign}\,(\zeta) = \pm 1$ on the left- and right-hand sides of the sheet when progressing along the sheet in positive s-direction, respectively. The tangential component of the velocity induced by the panel at its own midpoint experiences a jump across the panel of magnitude $\gamma(s_j^*)$, while the mean tangential velocity is non-zero if the panel has non-zero curvature. If the vortex distribution $\gamma(s)$ varies along the panel, also a mean normal velocity is induced at the panel midpoint. For a first-order panel method the last two terms are not present, since the panel curvature is not accounted for (i.e., $k_n(s_j^*) = 0$) and the vortex distribution is constant (i.e., $(d^2\Gamma/ds^2)(s_j^*) = 0$).

For points z_0 in the far field of a panel j, the expression for the velocity induced by the panel can be simplified. From Eq. (1) it follows that, consistent with the order of approximation considered, the velocity induced by panel j at points z_0 far away from $z(s_j^*)$,

$$v_j^*(z_0) = \frac{1}{2\pi i} \frac{\Delta s_j}{z_0 - z(s_j^*)} \left(\frac{d\Gamma}{ds}(s_j^*) \right). \tag{11}$$

2.2. Highly Rolled-up Regions

To preserve the accuracy of the approximation in regions of high curvature and regions of rapidly changing curvature, the panel size is decreased in some proportion to these quantities. To limit the total number of panels in regions where the vortex sheet rolls-up into a tight spiral, i.e., a vortex core, a model is used to represent such a region. The model could be a vortex patch ("finite core method") or a line vortex, connected to the end of the vortex sheet by a so-called "feeding sheet" as shown in Fig. 2 for the case of a single-branched vortex. If at other parts of the sheet the curvature increases above a critical value, indicative for the formation of a double-branched vortex, a line

vortex is introduced which replaces the highly rolled-up part of the vortex sheet. The line vortex is placed at the center of vorticity of the cutoff portion of the vortex sheet, and the circulation of the line vortex is equal to the circulation of the cutoff part of the sheet. In both single- and double-branched vortices the number of turns around the line vortex can be restricted to a user-specified angular extent while the rest of the sheet is amalgamated with the line vortex. The contribution of the line vortices to the velocity is given by

$$v_V^*(z_0) = \sum_{j=1}^{NV} \frac{1}{2\pi i} \frac{\Gamma_j}{z_0 - z_j}, \tag{12}$$

where NV denotes the number of line vortices. During the vortex sheet roll-up, parts of the vortex sheet are stretched, while other parts are compressed. As a result, the accuracy of the calculated induced velocity becomes non-uniform along the vortex sheet. In a similar way as has been proposed for the redistribution of the point vortices in the discrete vortex approach [14], a curvature-dependent rediscretisation scheme is used [12], which is governed by two parameters, namely a maximum permissible panel size $\Delta s_{\max}$ and a maximum permissible angular extent $\Delta\theta_{\max}/\tilde{k}_n$ where $\tilde{k}_n$, is the average curvature of the panel. The parameter $\Delta s_{\max}$ preserves the accuracy on flat and mildly curved parts of the sheet. The parameter $\Delta\theta_{\max}$ ensures that on a highly curved part of the sheet, the second-order accuracy of the induced velocity is maintained by reducing the panel size Δs_j in proportion to the magnitude of the curvature.

2.3. Implementation of the Normal-Velocity Boundary Condition

The condition of zero normal velocity at a solid boundary can be satisfied exactly by mirror-imaging the sources and vortices in the boundary. For simple geometries like an infinite wall or a circle, this is a feasible approach. For some more complex geometries it is possible to map the geometry in the physical domain onto a simpler geometry in a computational domain by a conformal transformation. In the computational domain the method of images can then be applied, to exactly satisfy the normal-velocity boundary condition on the imaginary axis. For a polygon this is accomplished by the Schwarz–Christoffel transformation of the polygon to a half plane (see Fig. 3). The transformation from the physical plane $z = x + iy$ to the computational plane $\zeta = \xi + i\eta$ is given by $z = f(\zeta)$, where

$$f'(\zeta) = K \prod_{i=1}^{NE} (\zeta - \zeta_i)^{\beta i/\pi} \tag{13}$$

and the prime denotes the derivative with respect to ζ while the angle β_i is given in Fig. 3. The parameter K is a complex-valued constant and the product is taken over all edge points (NE) of the polygon. While the derivative of the transformation function $f(\zeta)$ can be found for any polygon, often the function $f(\zeta)$ itself and the inverse transformation cannot be obtained in algebraic form.

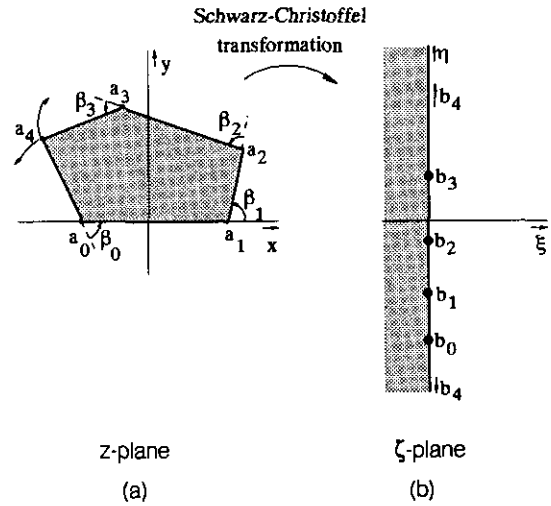

FIG. 3. Schwarz–Christoffel transformation of the inside of a polygon onto a semi-plane: (a) physical plane $z = x + iy$; (b) computational plane $\zeta = \xi + i\eta$.

When analytical solutions of the transformation function are not available, numerical procedures to find the Schwarz–Christoffel transformation function can be used [15].

Since the transformation is conformal, the complex potential in the computational plane is equal to its value at the corresponding position in the physical plane and if the normal velocity boundary condition is satisfied in the computational plane, it is also satisfied in the physical plane. The complex potential is defined as $\Phi = \phi + i\psi$, where ϕ and ψ are the velocity potential and stream function, respectively. The complex potential is in the computational plane given by

$$\Phi(\zeta) = \sum_{j=1}^{NV} \frac{\Gamma_j}{2\pi i} \ln\left(\frac{\zeta - \zeta_j}{\zeta + \zeta_j^*}\right) + \sum_{j=1}^{NP} \int_{s_j}^{s_{j+1}} \frac{1}{2\pi i} \ln\left(\frac{\zeta - \zeta_j(s)}{\zeta + \zeta_j^*(s)}\right) d\Gamma(s) \tag{14}$$

which consists of contributions of the continuous vortex sheet, the line vortices, and the image vortex system. The velocity $v^*(z) = (d\Phi/dz)(z)$ in the physical plane, at a point where the velocity is not singular, can be obtained from the complex velocity potential $\Phi(\zeta)$ in the computational plane as

$$\frac{d\Phi}{dz}(z) = \frac{d\Phi}{d\zeta}(\zeta)/f'(\zeta). \tag{15}$$

However, at the position of the line vortex, where the complex

potential is singular, an additional term arises due to the transformation, which is known as Routh's correction [16]; e.g., the velocity at a point $z = z_v$, where a point vortex of circulation Γ_v is located, is

$$\frac{d\Phi}{dz}(z_v) = \lim_{\zeta \to \zeta_v} \underbrace{\left(\frac{d\Phi}{d\zeta}(\zeta) + \frac{i\Gamma_v}{2\pi} \frac{1}{\zeta - \zeta_v} \right)}_{\text{regular part of } d\Phi/d\zeta} / f'(\zeta_v) + \underbrace{\frac{i\Gamma_v}{4\pi} f''(\zeta_v)/(f'(\zeta_v))^2}_{\text{Routh's correction}} \tag{16}$$

with ζ_v the position of the line vortex in the ζ-plane.

The boundary conditions on a vortex sheet are that the vortex sheet is a stream surface, i.e., $\Im(v(z)(dz^*/ds)) = 0$ and that the vortex sheet cannot sustain any forces, so that the pressure difference across the sheet is zero, i.e., $\rho(\partial\varphi/\partial t) + \frac{1}{2}\rho|\nabla\varphi|^2$ is identical on both sides of the sheet. Combining the two conditions shows that the vorticity once generated at a sharp edge is convected with the mean local flow velocity, or

$$\frac{dz^*(s)}{dt} = \frac{d\Phi}{dz}(z(s)), \quad \frac{d\Gamma(s)}{dt} = 0. \tag{17}$$

The velocity with which the vortex sheet convects in the computational plane is obtained from the complex velocity potential Φ and the transformation function $f(\zeta)$ as

$$\begin{aligned} \frac{d\zeta(s)}{dt} &= \frac{dz(s)}{dt} \frac{1}{f'(\zeta(s))} \\ &= \left(\frac{d\Phi}{d\zeta}(\zeta(s)) \right)^* \left| \frac{1}{f'(\zeta(s))} \right|^2, \end{aligned} \tag{18}$$

where the first derivative of the complex potential Φ in the computational plane is obtained as described in Section 2.1.

In the computational plane, the line vortex is convected like

$$\frac{d\zeta_v}{dt} = \left\{ \lim_{\zeta \to \zeta_v} \left(\frac{d\Phi}{d\zeta} + \frac{i\Gamma_v}{2\pi} \frac{1}{\zeta - \zeta_v} \right) + \frac{i\Gamma_v f''(\zeta_v)}{4\pi f'(\zeta_v)} \right\}^* \left| \frac{1}{f'(\zeta_v)} \right|^2. \tag{19}$$

This implies that the first and second derivatives of the transformation function $f(\zeta)$, not the function itself, are required to calculate the convection of the vortex system in the computational plane.

The time dependent position of the vortex sheet is found by integrating in time the convection velocity of the vortex sheet panels and line vortices. In the vortex-sheet method the integration in time is performed by a first-order explicit Euler scheme, with an adaptive timestep Δt. The time step is adapted by restricting it such that each panel is displaced not more than a fraction of its length.

2.4. Generation of Vorticity

In actual flows, due to the action of viscous forces, vorticity is generated at solid boundaries. In a high-Reynolds-number flow, the region with rotational flow is mostly limited to a thin boundary layer along the solid boundary. However, at sharp corners or on a strongly curved part of the wall, the boundary layer can separate from the wall. The vorticity contained in the boundary layer leaves the surface and a free shear layer is formed. In any inviscid model of the flow separation and the associated generation of vorticity is to be included explicitly through a Kutta condition.[1] The Kutta condition requires the velocity to remain finite at sharp edges. Since the velocity is given by Eq. (15) and since at sharp edges ($\zeta = \zeta_s$) the derivative of the transformation function $f'(\zeta)$ is zero, the Kutta condition requires that

$$\frac{d\Phi}{d\zeta}(\zeta_s) = 0. \tag{20}$$

This implies that in the physical plane the flow must separate at the edge with a finite velocity.

In an unsteady potential flow the Kutta condition cannot be fulfilled in general without introducing vorticity in the flow. The velocity induced by the shed vorticity removes the singular behavior of the potential flow around the edge, and a finite velocity at the edge remains.

The present computational procedure, implemented in the computational ($\zeta-$) plane, consists of six subsequent sub-steps.

1. Given the position $\zeta(s;t)$ and dipole strength $\Gamma(s;t)$ as a function of the arc length s along the vortex sheet at time t, cubic spline interpolations are set up based on values of ζ and Γ at discrete points s_j for $j \in [1, ..., NP + 1]$, where $NP + 1$ is the number of discrete points.

2. A new panel distribution $\hat{s}_j$ for $j \in [1, ..., NP + 1]$ with NP the number of panels is determined by an adaptive curvature-dependent re-paneling scheme, aimed at preserving the second-order accuracy in space of the panel method. Also, if a strong variation of the transformation function $z = f(\zeta)$ occurs on a part of the vortex sheet, the panel size is reduced, which limits the panel width in regions in the physical plane strongly stretched by the Schwarz–Christoffel transformation, i.e., near edges. In the adaptive scheme the panel size is further limited to a maximum value $\Delta s = \min(\Delta s_{\max}, \Delta\theta_{\max}/\tilde{k}_n)$, where $\tilde{k}_n$ is the average curvature of the panel and $\Delta\theta_{\max}$ is the maximum angle subtended by a single panel. The panel size in the physical plane is also limited to $\Delta s_{\max}$. The angular extent θ_v of the vortex sheet spiraling around the line vortex representing the vortex core can be limited. The part of the vortex sheet that exceeds the specified angular extent θ_v is amalgamated with the line vortex. In this amalgamation procedure, carried

[1] Sometimes referred to as the Kutta–Joukowski condition.

out in the physical plane, the center of vorticity of the line vortex before amalgamation and the part of the vortex sheet that has been cut off is conserved. The result at this sub-step is that we have the position $\zeta(\hat{s}_j; t)$ and the dipole strength $\Gamma(\hat{s}_j; t)$ for $j \in [1, ..., NP + 1]$ at the edge points of the individual panels. Note that NP is not necessarily equal to *NP*; i.e., the number of panels is allowed to increase in response to the needs of the adaptations.

3. The derivative of the complex potential at the panel midpoints, i.e., $\zeta(\tilde{s}_j; t)$ for $j \in [1, ..., NP]$, is computed using the second-order panel method operating on the vortex sheet in the computational plane. This complex velocity, computed from Eqs. (7) and (12) with z replaced by ζ consists of the free stream velocity, the velocity induced by the dipole panels and the velocity induced by the line vortices. Substituting the derivative of the potential with respect to ζ in the right-hand side of Eq. (19), the rate at which the position of the vortex sheet advances in time is obtained. Similarly, the velocity at the line vortex is used to compute the right-hand side of Eq. (19), which includes Routh's correction.

The displacement of the beginning and ending points of the vortex sheet are derived from a quadratic extrapolation of $d\Phi/d\zeta$, using the values at the first and last three midpoints on the vortex sheet, respectively. However, if the edge point is connected to the sharp edge, where the Kutta condition is to be imposed, the extrapolation of the velocity is performed in the physical plane, rather than in the computational plane. The reason is the following. The Kutta condition, given by Eq. (20), requires the derivative of the complex potential in the ζ-plane to be zero; however, it tends to zero in a non-polynomial fashion, i.e., with the second derivative becoming infinite at the edge. An accurate extrapolation requires knowledge on the behaviour of $\Phi(\zeta)$ near the edge. However, $d\Phi/dz$ on the vortex sheet near the edge in the physical $(z-)$ plane is finite; i.e., vorticity convects away from the edge with a finite and more regularly behaving velocity, enabling a more accurate extrapolation.

4. The new position of the midpoints of the panels, that of the first and last edge points of the vortex sheet, and that of the line vortices is found by application of the first-order Euler scheme, e.g.,

$$\zeta(\tilde{s}_j; t + \Delta t) = \zeta(\tilde{s}_j; t) + \frac{d\zeta}{dt}(\tilde{s}_j; t)\Delta t, \quad j = 1 \ldots \text{NP}. \quad (21)$$

The convection procedure is illustrated in Fig. 4. The time step in the Euler scheme, used for the convection of the panel midpoints, the first and the last points of each vortex sheet, and the line vortices, is adaptive, in that the time step Δt is limited such that it does not exceed Δt_{max} and simultaneously such that none of the midpoints $\zeta(\tilde{s}_j; t)$ is displaced more than a specified fraction $\mathcal{F}$ of its own width in terms of the arc length or more than a certain maximum displacement Δx_{max}. The parameters Δx_{max}, Δt_{max}, and $\mathcal{F}$ are to be chosen such that

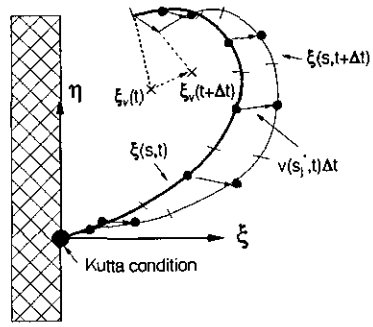

FIG. 4. *Convection of the point vortices and the vortex sheet, only midpoints and first and last edge points of the continuous vortex sheet segment are convected. In case the vortex sheet is connected to the wall, at each time step a new panel is introduced reconnecting the edge point and the first convected edge point.*

the accuracy of the time integration is preserved in time and also such that it is in balance with the spatial accuracy.

5. The gap between the edge and the convected first point of the vortex sheet constitutes a new panel. The "bridging" panel is not necessarily directed tangentially to either side of the sharp edge. The dipole strength $\Gamma(0; t + \Delta t)$ at the edge is determined from the application of the Kutta condition that in the computational plane $d\Phi/d\zeta$ (ζ_s) due to the vortex system in its new position vanishes at the edge.

6. The location $\zeta(\hat{s}_j; t + \Delta t)$ of the panel edge points at time $t + \Delta t$ is computed by a quadratic spline, fitted through the location $\zeta(\tilde{s}_j; t + \Delta t)$ of the panel midpoints at time $t + \Delta t$. The value of the dipole strength $\Gamma(\hat{s}_j; t + \Delta t)$ at time $t + \Delta t$ at the panel edge points equals the value at time t; i.e., the dipole strength is convected with the sheet.

This completes one cycle of the computational procedure. Steps 1 through 6 are repeated until the specific number of timesteps has been carried out or until a panel becomes smaller than a given minimum length.

3. APPLICATIONS

3.1. Starting Flow Past a Wedge

As a first application of the method the impulsively started flow around an infinite wedge is considered. The flow separates at the sharp edge of the wedge and the vorticity generated at the edge convects with the local flow velocity away from the edge into the flow field. For the high Reynolds number considered, the vorticity remains concentrated in a relatively thin free shear layer emanating from the edge, across which a rapid variation in tangential velocity takes place. Further away from the edge the free shear layer rolls up into a vortical core. Within the core the vorticity is spatially distributed in a smooth fashion with a maximum at the center of the vortex core. In the core, the individual turns of the spiraling free shear layer cannot be

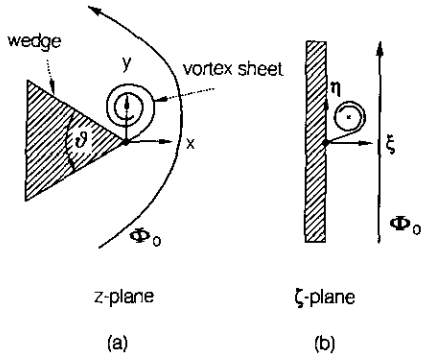

FIG. 5. Schwarz Christoffel transformation of a wedge: (a) physical plane $z = x + iy$; (b) computational plane $\zeta = \xi + i\eta$.

identified anymore. In the potential-flow model of the flow the shear layer is assumed to be infinitesimally thin with all the vorticity contained in this vortex sheet.

Because there is no length or time scale involved the resulting potential flow problem has a self-similar solution in which the shape and strength of the vortex sheet are stationary in terms of self-similar variables [17]. However, the computational method is applied in the time-domain and the method is validated by checking whether for large times the self-similar solution is attained.

By conformal transformation the flow domain in the physical plane $z = x + iy$ is mapped onto a half-plane $\xi > 0$ in the computational plane $\zeta = \xi + i\eta$ (see Fig. 5). The mapping is given by $z = f(\zeta)$, where

$$f(\zeta) = (\zeta/D)^{1/n} \tag{22}$$

with

$$n = \pi/(2\pi - \theta)$$

and D is a complex constant while the value of n is determined by the included angle θ of the wedge and varies between $n = 0.5$, for the included angle $\theta = 0$ (flat plate) and $n = 1$ for $\theta = \pi$ (smooth wall).

The attached potential flow around the edge is described by the complex potential

$$\Phi_0(\zeta) = -iA\zeta, \tag{23}$$

where A is a real constant.

In case the flow separates at the edge the velocity potential at a point ζ in the computational plane is a superposition of the onset flow $\Phi_0(\zeta)$ given by Eq. (23) and the flow induced by the vortex sheet $\Phi_s(\zeta)$; i.e.,

$$\Phi_s(\zeta) = \frac{1}{2\pi i}\int_0^{s_{tot}} \gamma(s)\ln\left(\frac{\zeta - \zeta_s(s)}{\zeta + \zeta_s^*(s)}\right)ds, \tag{24}$$

where $\gamma(s) = -d\Gamma/ds$ is the vortex distribution and the integration is along the vortex sheet $\zeta = \zeta_s(s)$, with $s_{tot} \to \infty$. Note that the boundary condition on the surface of the wedge in the computational plane ($\xi = 0$) is satisfied by mirror-imaging the vortex system in the positive half-plane into the vertical plane. The circulation along the sheet is defined as the jump in the value of the velocity potential across the sheet. At a point s of the sheet it can be determined from

$$\Gamma(s) = -\int_s^{s_{tot}} \gamma(s^*)ds^*, \tag{25}$$

where the integral is taken from the point s on the sheet to the endpoint of the rolled-up vortex sheet. The circulation contained within the vortex sheet is $\Gamma(0)$, which corresponds to the value of the dipole strength at $s = 0$, i.e., the location where the sheet is connected to the edge of the wedge.

The velocity at a point z in the physical plane is given by Eq. (15) applied to the complex potential $\Phi(\zeta) = \Phi_0(\zeta) + \Phi_s(\zeta)$. Using Eqs. (22), (23), and (24) we obtain

$$\left(\frac{d\Phi}{dz}\right)(z) = \left[-iA + \frac{1}{2\pi i}\int_0^{s_{tot}} \gamma(s)\left(\frac{1}{\zeta - \zeta_s(s)} - \frac{1}{\zeta + \zeta_s^*(s)}\right)ds\right] nD^{1/n}\zeta^{1-1/n}, \tag{26}$$

where the integral is taken over the whole vortex sheet.

To obtain the velocity at a point $\zeta = \zeta_s$ on the vortex sheet the Cauchy principal value of the integral in Eq. (26) should be taken.

The Kutta condition requires that the singular behavior of the velocity field due to $\Phi_0(\zeta)$ at the edge $\zeta = 0$ is compensated by the velocity induced by the vortex sheet (see Eq. (20)). Using Eq. (26) one finds

$$A = \frac{1}{2\pi}\int_s^{s_{tot}} \gamma(s)\left(\frac{1}{\zeta_s(s)} + \frac{1}{\zeta_s^*(s)}\right)ds. \tag{27}$$

TABLE I

Parameters Used for the Application of the Vortex-Sheet Method to the Starting Flow around a Wedge with $\theta = 90°$ (see Fig. 6)

Time step	δ	Δs_{max}	$\Delta\theta_{max}$	θ_v
1–250	0.2	0.05	15°	180°
251–350	0.2	0.10	20°	1620°
351–550	0.2	0.05	15°	1620°
551–3550	0.2	0.04	15°	1620°

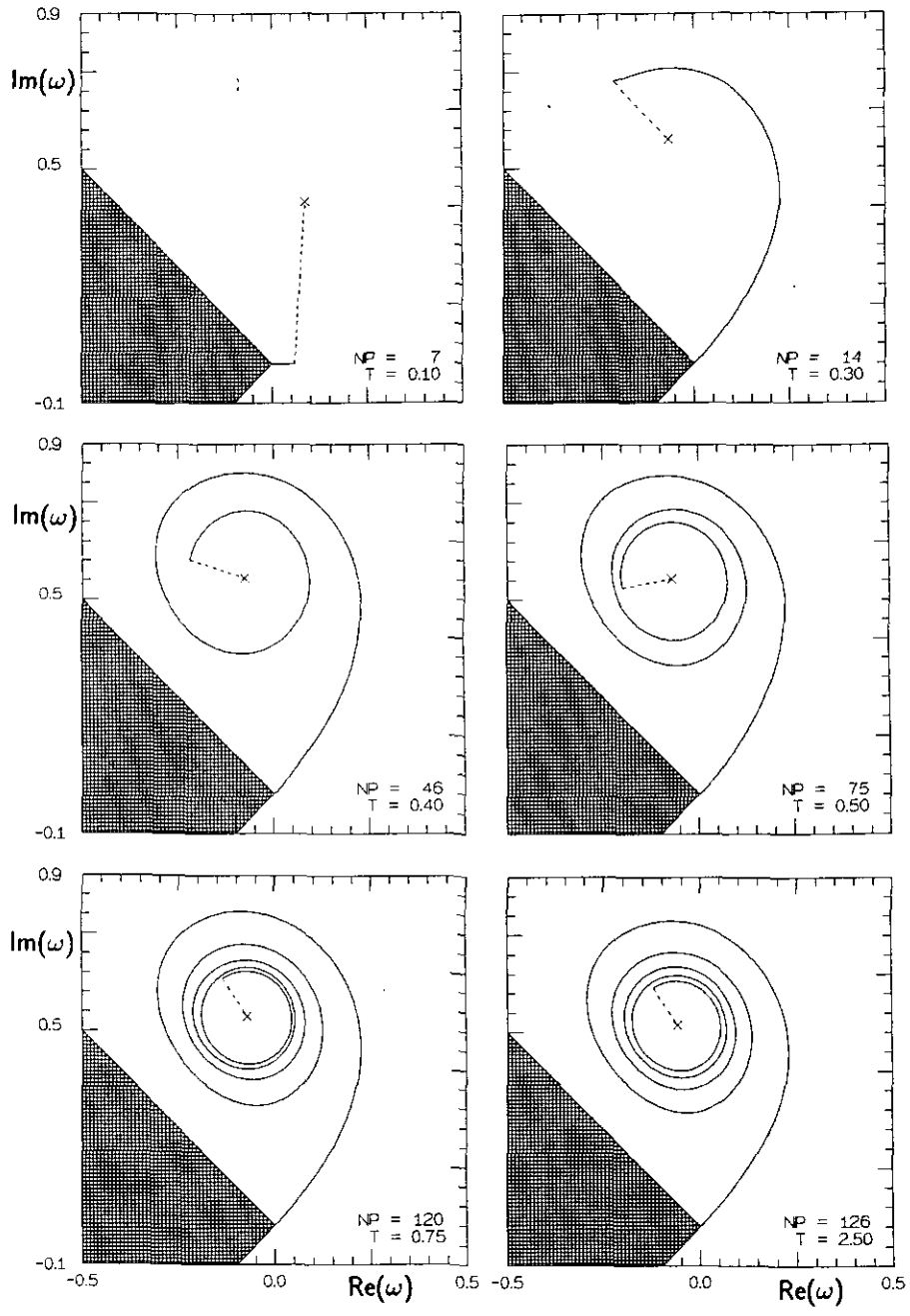

FIG. 6. Impulsively started flow around a 90° infinite wedge. Development of the vortex sheet computed in the time domain with the vortex-sheet method. The vortex sheet geometry is given in similarity coordinates $\omega(\lambda)$. The time-invariant similarity solution is obtained at $t = 2.5$.

The time-scaled similarity variables are related to the coordinates and the circulation of the vortex sheet [17] as

$$z = ((2-n)(1-n)AD t)^{1/(2-n)}\omega(\lambda)$$
$$\Gamma(0) = ((2-n)(1-n)t)^{n/(2-n)}(AD)^{2/(2-n)}J, \qquad (28)$$

respectively. Here $\omega(\lambda) = \rho(\lambda)\, e^{i\chi(\lambda)}$ and J are the self-similarity coordinates and the scaled circulation, respectively. The parameter λ is one minus the scaled circulation along the vortex sheet and it is zero at the edge and one at the end of the vortex sheet. If $\Gamma(s)$ is a monotone function of the arc length s along the vortex sheet, λ can be used as an independent variable along the vortex sheet,

$$\lambda(s) = 1 - \frac{\Gamma(s)}{\Gamma(0)}. \qquad (29)$$

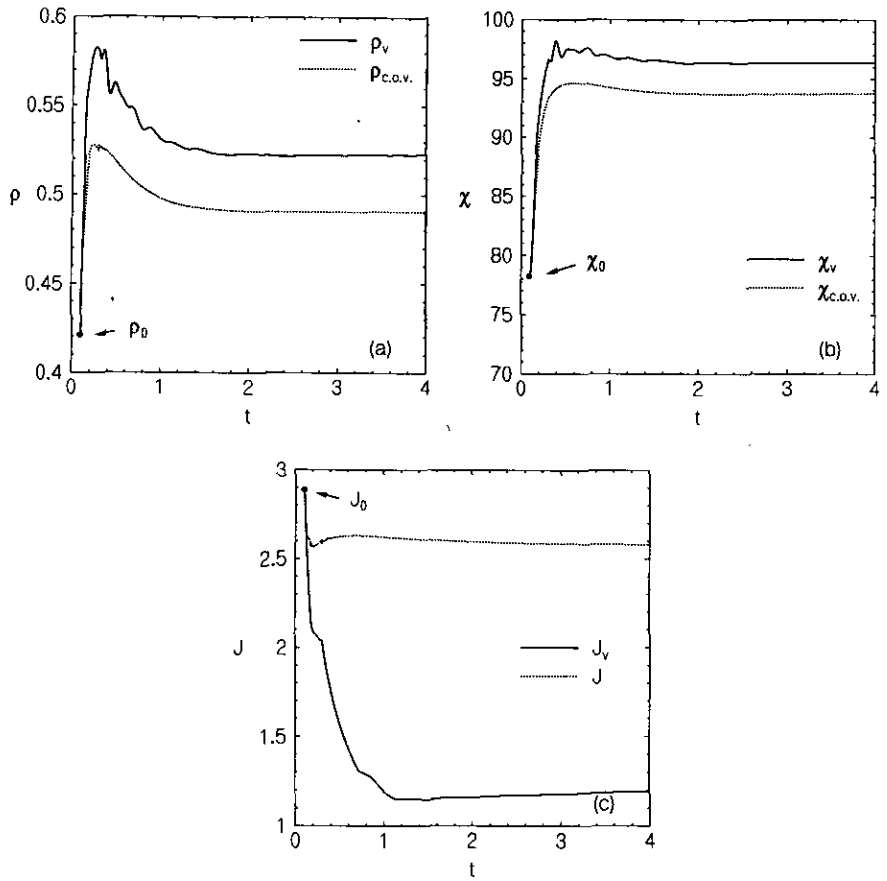

FIG. 7. Impulsively started flow around a 90° infinite wedge. Vortex position $\omega_v = \rho_v e^{i\chi_v}$, center of vorticity $\omega_{c.o.v.} = \rho_{c.o.v.} e^{i\chi_{c.o.v.}}$, line vortex strength J_v and circulation J, in similarity variables, converge to a time-invariant self-similar solution. The single vortex solution $\omega_0 = \rho_0 e^{i\chi_0}$, J_0 [18], given by Eq. (30) with $n = \frac{2}{3}$ and $\Lambda = \frac{3}{5}$, is used as a start for the iteration procedure.

Equations (17), (26), and (27) rewritten in terms of similarity variables form a single, time-independent system of nonlinear equations, which has to be solved iteratively. Pullin [17] solved the problem of the starting flow around a wedge formulated in the similarity variables numerically employing a Newton–Raphson scheme. He discretised the portion of the vortex sheet attached to the edge by a number (75) of segments. The rolled-up part of the vortex sheet is represented by a line vortex. The method requires an initial solution from which the iterative procedure is started. To this purpose the single-vortex solution [18] is utilized, in which the vortex sheet is omitted. This solution gives the vortex position $z_v = \rho_v e^{i\chi_v}$ and vortex strength J as

$$\begin{aligned} \rho_v &= \left(n\sqrt{1 - 1/(4n)}\,\Lambda\right)^{1/(2-n)} \\ \chi_v &= \frac{1}{n}\arccos\left(\frac{1}{2\sqrt{n}}\right) \\ J &= 2\pi\sqrt{n}\rho_v^n, \end{aligned} \tag{30}$$

where the value of Λ depends on the type of condition imposed on the vortex system [19]. The "force free" condition, proposed by Brown and Michael [20], corresponds to the value of $\Lambda = 1/(n + 1)$.

Pullin [17] started the solution of the problem by first considering the flow around a semi-infinite flat plate ($n = \frac{1}{2}$). The streakline of the flow emanating from the edge is taken as the initial position of the vortex sheet which is iteratively improved upon. Subsequently the solution for the flat plate was used as an initial guess for the solution of the flow around wedges with nonzero included angle ($\frac{1}{2} < n < 1$). For a flow past a wedge with interior angle of 90° ($n = \frac{2}{3}$) Pullin [17] obtained for the circulation the value $J = 2.53$ and for the scaled position of the core vortex, $\omega_v = \rho_v e^{i\chi_v}$, $\rho_v = 0.54$, and $\chi_v = 98°$. The circulation of the line vortex representing the vortex core took the value $J_v = 1.09$.

In the present method the vortex sheet is divided into NP panels while the highly rolled-up part of the vortex sheet is represented by a line vortex. The complex potential at a point

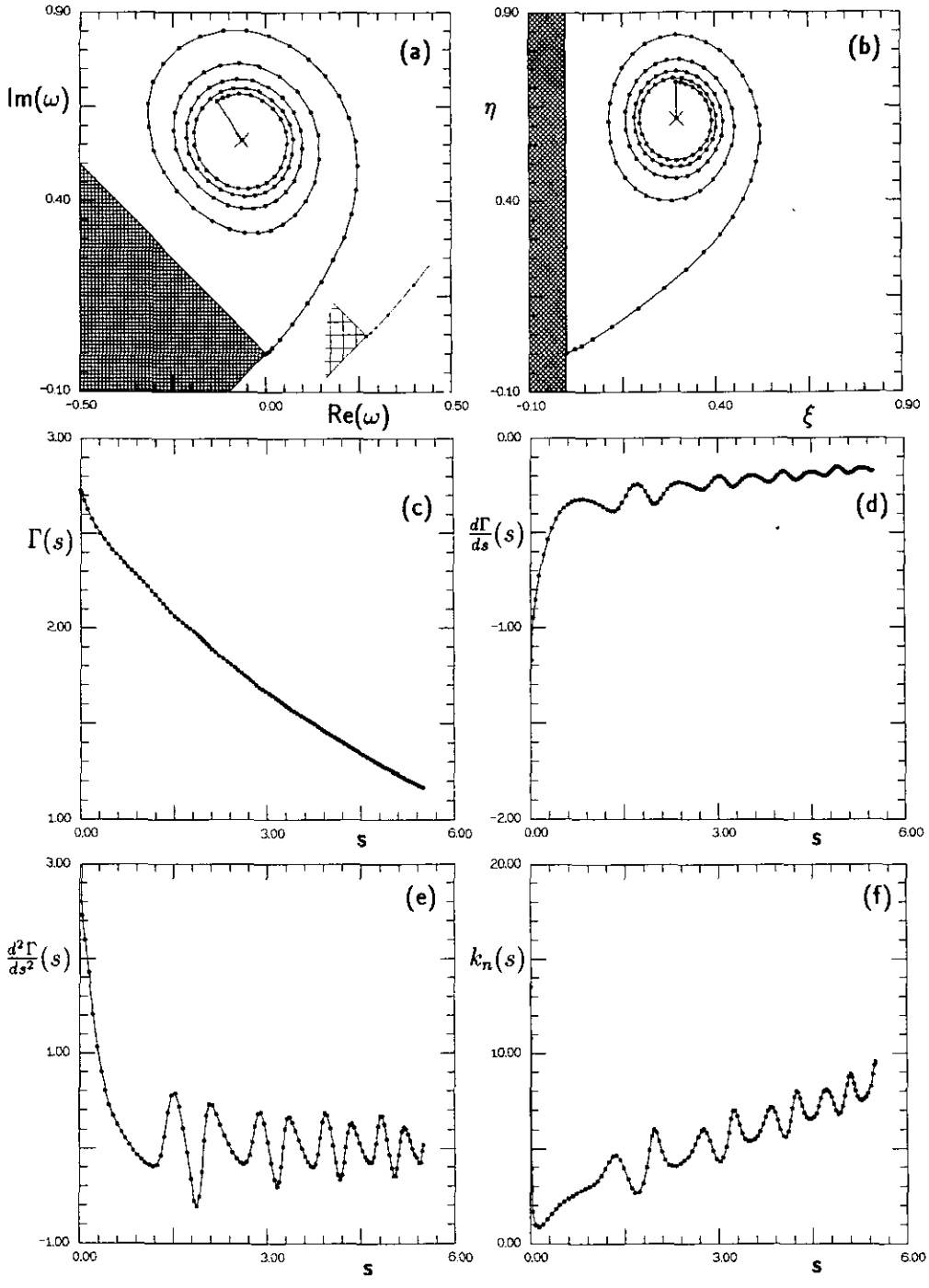

FIG. 8. Characteristics of the solution presented in Fig. 6 at $t = 2.5$: (a) vortex sheet in physical plane, with enlargement of the region near the edge (o = edge points of the panels); (b) vortex sheet in computational plane; (c) dipole distribution $\Gamma(s)$; (d) vortex distribution $d\Gamma(s)/ds = -\gamma(s)$; (e) derivative of vortex distribution $d^2\Gamma(s)/ds^2$; (f) curvature $k_n(s)$; (c–f) are expressed in terms of the physical plane.

ζ in the computational plane due to the line vortex at position ζ_v and the mirror imaged vortex at $\zeta = -\zeta_v^*$ is given by

$$\Phi_v(\zeta) = \frac{\Gamma_v}{2\pi i} \ln\left(\frac{\zeta - \zeta_v}{\zeta + \zeta_v^*}\right), \tag{31}$$

where Γ_v is the circulation of the line vortex.

The complex potential is now given by summing all the contributions,

$$\Phi(\zeta) = \Phi_0(\zeta) + \Phi_s(\zeta) + \Phi_v(\zeta), \tag{32}$$

where $\Phi_0(\zeta)$ is the attached flow component given by Eq. (23), $\Phi_s(\zeta)$ is the potential due to the continuous parts of the vortex sheet, Eq. (24), and $\Phi_v(\zeta)$ is the potential due to the line vortices, Eq. (31).

The initial solution, for $t \leq t_1$, is formed by the line vortex at the location given by Eq. (30) with $n = \frac{2}{3}$, $\Lambda = \frac{3}{5}$ and a flat vortex sheet segment of constant dipole strength $\Gamma(s) = J$ situated along the extension of the bisector of the wedge. The vortex sheet, discretised into five panels, starts to convect with the flow and to gain in circulation through the new vorticity introduced by the application of the Kutta condition at the edge.

The results of this simulation in the time domain will be presented in terms of the similarity variables $\omega(\lambda)$ and J for the position of the vortex system and its circulation, respectively. The parameters used for the vortex-sheet calculation are given in Table I. Proceeding in time a time-invariant similarity solution is reached (see Fig. 6). Following the initial stage with a smaller fixed angle θ_v, a number of time steps have been performed with a larger value of $\Delta s_{\max}$ and $\theta_{\max}$, in order to damp out spurious initial disturbances in the vortex sheet geometry. In Fig. 7 the vortex position and strength are given as a function of time. For $t \leq t_1 = 0.1$ the values are given by the single vortex solution, Eq. (30). Clearly, for the time-invariant solution, the position of the center of vorticity differs significantly from the point vortex position, both in terms of the distance to the edge and the angle. Comparing the converged solution with the results obtained by Pullin [17] we observe only slight differences. The present solution for the position of the core vortex is $\rho_v = 0.52$ and $\omega_v = 96.6°$, while the circulation of the vortex system is $J = 2.58$ and that of the line vortex is $J_v = 1.12$. The results differ less than 4% from the results obtained by Pullin [17]. Results obtained for the starting flow past a flat plate ($\theta = 0°$, $n = \frac{1}{2}$) are even in closer agreement with the results found by Pullin [17] and are reported by Peters [19].

Figure 8 presents for the solution at $t = 2.5$ the position of the vortex sheet in the computational and physical planes. Figure 8 also gives the dipole distribution and the first and second derivatives of the dipole distribution along the sheet

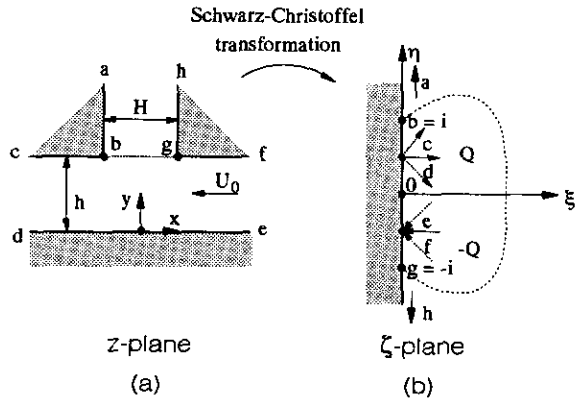

FIG. 9. Conformal mapping of region within a T-junction to a half plane.

with respect to the arc length s and the curvature of the sheet, all in the physical plane. At the edge the direction of the first derivative of the position vector corresponds with the tangent along the lower side of the wedge. Note that this is not explicitly imposed in the present numerical scheme. Application of the Kutta condition results in a vortex sheet leaving the wedge tangentially. Regions of high curvature k_n correspond with regions of high values of the vortex strength $\gamma(s)$. Figure 8 shows that even in the tightly rolled-up region the vortex sheet appears to keep an elliptical shape, since the value of $k_n(s)$ keeps oscillating even close to the vortex core.

At the edge the curvature shows a singular behavior; it *tends to infinity* at the edge. The singular behavior of the vortex sheet near the edge has already been hypothesized [21, 22], proposing that the vortex sheet near the edge should behave as $y_n = Cx_\tau^{3/2}$, where x_τ and y_n are coordinates parallel and normal to the lower side of the wedge, respectively. The present vortex-sheet solution appears to confirm the singular behavior.

3.2. Starting Flow in a T-Junction

In order to assess the applicability of the method to flows in pipe systems, we consider the inviscid, incompressible starting flow in a channel with a two-dimensional T-junction between a main pipe of width h and a deep cavity. The T-junction has sharp edges and the width of the side branch is H (see Fig. 9). Since the side branch is closed, the volume flux, per unit length in the third dimension, is directed through the main pipe. The coordinate z, the volume flux $Q = U_0 h$, time t, circulation Γ, the main pipe width h, and the complex velocity potential are non-dimensionalised with U_0 and H according to

$$\begin{aligned} z &= z^* H, \qquad t = t^* H/U_0 \\ Q &= Q^* U_0 H, \quad h = h^* H \\ \Gamma &= \Gamma^* U_0 H, \quad \Phi = \Phi^* U_0 H. \end{aligned} \tag{33}$$

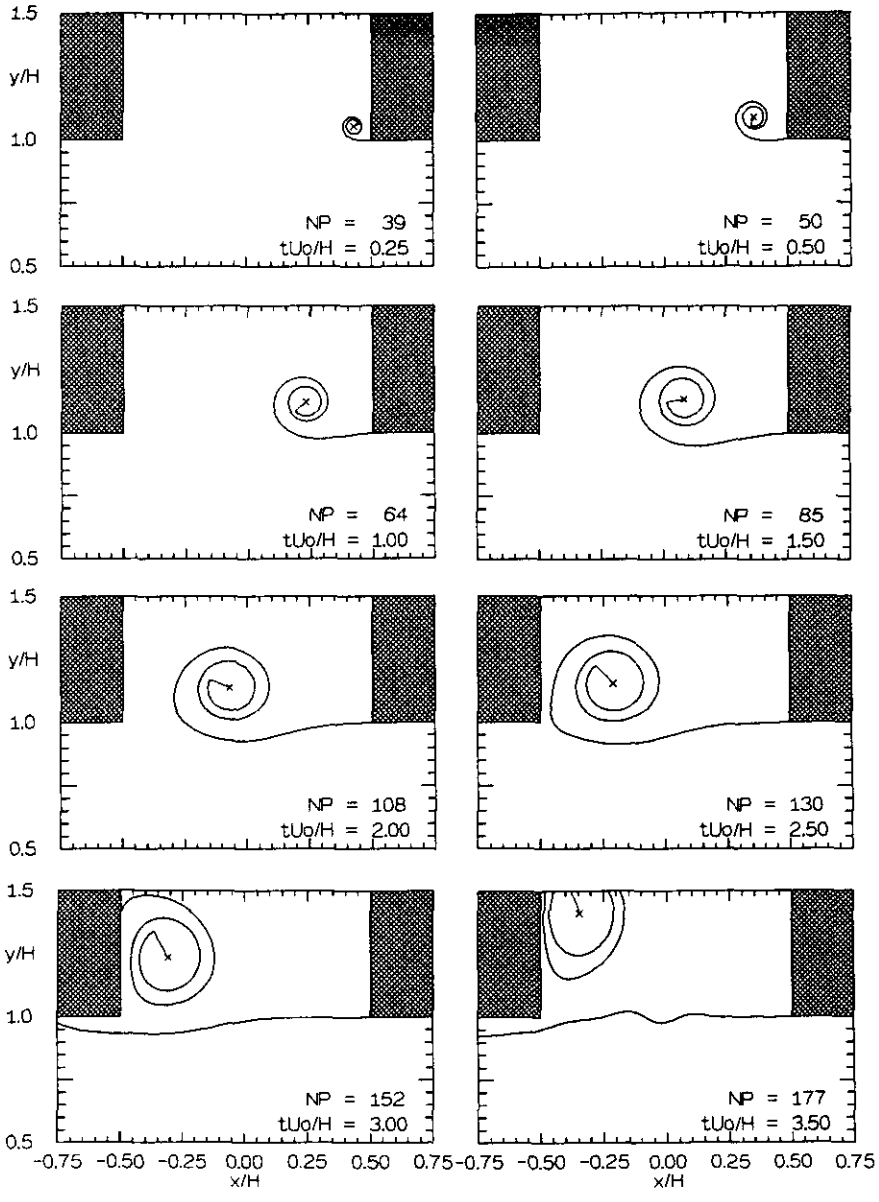

FIG. 10. Impulsively started flow in a T-junction computed with the vortex-sheet method.

In the sequel the non-dimensionalised quantities will be used and the asterisk will be omitted. For the purpose of easily satisfying the boundary conditions on the solid walls the inner part of the T-junction in the physical plane ($z = x + iy$) is mapped to the half plane $\Re(\zeta) > 0$ in the computational plane ($\zeta = \xi + i\eta$) as shown in Fig. 9. This is accomplished by the conformal mapping $z = f(\zeta)$ with

$$f'(\zeta) = \frac{ih}{\pi}\frac{\sqrt{\zeta^2 + 1}}{\zeta^2 + a^2}, \tag{34}$$

where $a = 1/\sqrt{1 + 4h^2} < 1$. The transformation is obtained from Eq. (34) by integration as

$$f(\zeta) = \tfrac{1}{2} + ih + \frac{i}{\pi}\ln\left(i\zeta + \sqrt{-\zeta^2 - 1}\right) - \frac{h}{\pi}\ln\left(\frac{i\zeta - a}{i\zeta + a}\right) - \frac{2h}{\pi}\ln\left(\frac{\sqrt{(1-a)(i\zeta - 1)} + i\sqrt{(1+a)(i\zeta + 1)}}{\sqrt{(1+a)(i\zeta - 1)} + i\sqrt{(1-a)(i\zeta + 1)}}\right). \tag{35}$$

The upstream and downstream edges of the T-junction are mapped onto $\zeta = -i$ and $\zeta = i$, respectively. Upstream infinity ($x = \infty$) is mapped onto $\zeta = -ia$; downstream infinity ($x = -\infty$) is mapped onto $\zeta = ia$. The uniform flow at infinity, with velocity U_0 is generated by a point source of strength $Q = 2h$ at $\zeta = -ia$ and a sink of equal strength at $\zeta = ia$. The dotted

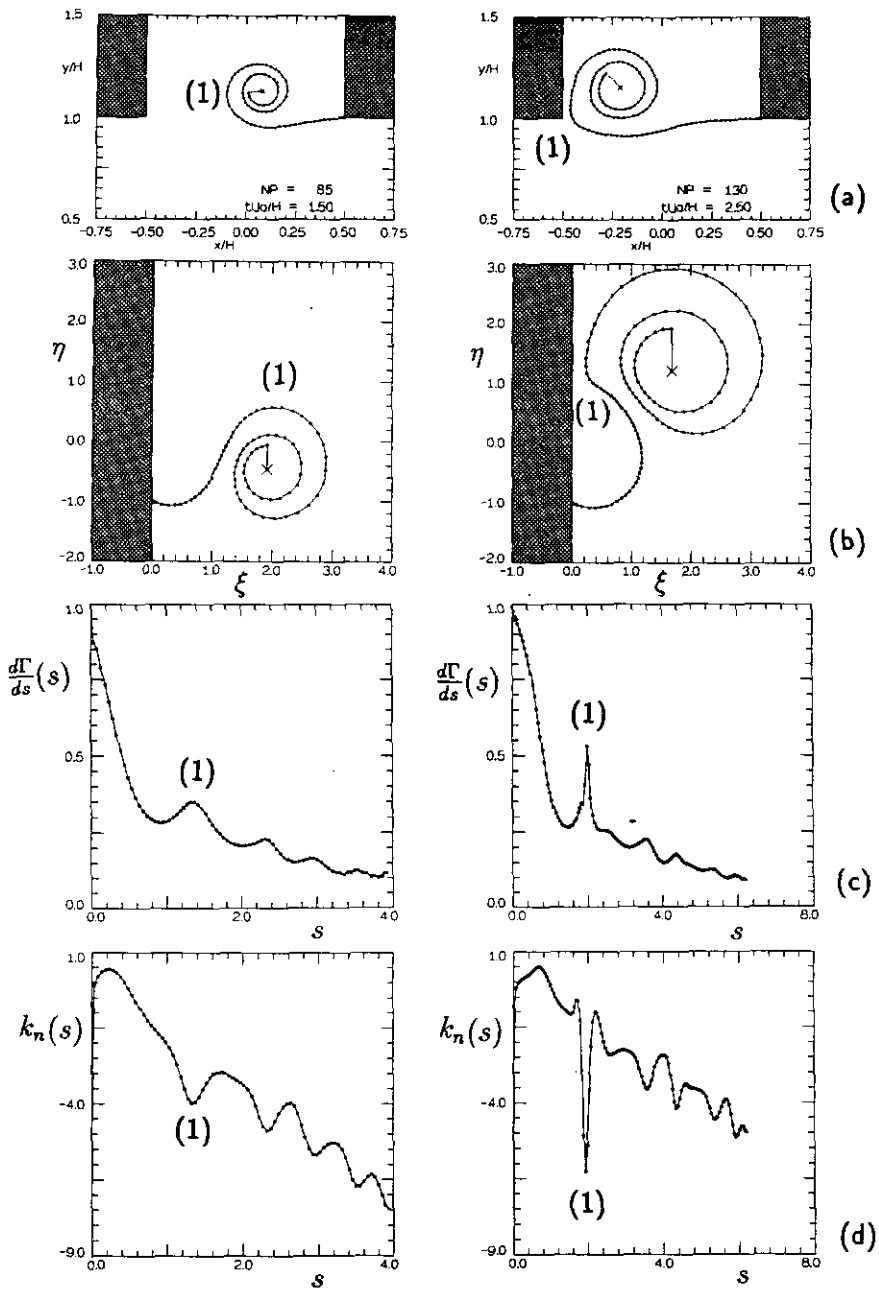

FIG. 11. Characteristics of the vortex-sheet solution presented in Fig. 10 at $tU_0/H = 1.5$ (left column) and $tU_0/H = 2.5$ (right column): (a) solution in physical plane (o denote edge points of the panels); (b) solution in the computational plane; (c) vortex distribution $d\Gamma/ds(s) = -\gamma(s)$; (d) curvature $k_n(s)$.

line in Fig. 9 indicates the intersection between the side branch and the main pipe, both in the computational plane as well as in the physical plane. The complex potential due to the attached main flow is given by

$$\Phi_0(\zeta) = \frac{h}{\pi} \ln\left(\frac{\zeta + ia}{\zeta - ia}\right). \tag{36}$$

As a result of the action of viscosity the flow separates at the sharp upstream edge and vorticity is generated continuously at the edge and convected into the flow field. At the downstream sharp edge it has been observed by means of flow visualization that separation does not take place or is of limited extent [19]. Therefore in the numerical simulations only flow separation at the upstream edge is taken into account.

For the initial stage of the development of the flow, when the separated flow region is still small compared to the side branch width H, the position of the tightly rolled-up vortex

TABLE II

Parameters Used for the Application of the Vortex-Sheet Method to the Starting Flow in a T-Junction (see Fig. 10)

Time step	$\tilde{\sigma}$	Δs_{max}	$\Delta\theta_{max}$	θ_v
1–250	0.2	0.01	20°	225°
251–500	0.2	0.02	20°	360°
501–1000	0.3	0.05	20°	540°
1001–4000	0.3	0.05	20°	900°

sheet and its circulation can be estimated by a self-similar solution of the flow past an infinite wedge with the interior angle equal to the included angle of the upstream edge, i.e., $\theta = 90°$. Near the upstream edge ($z = \frac{1}{2} + ih$, $\zeta = -i$) the transformation function given in Eq. (35) can be approximated by

$$z - \tfrac{1}{2} - ih = \frac{2\sqrt{2}h}{3\pi(1-a^2)}(-i)^{3/2}(\zeta + i)^{3/2} \tag{37}$$

and the expression for the attached-flow velocity potential (36) to

$$\Phi_0 H_{\zeta \to -i} = \frac{2iah}{\pi(1-a^2)}(\zeta + i) + \cdots. \tag{38}$$

The self-similar problem of a starting flow past the wedge can be defined according to Eqs. (22) and (23) with parameters

$$D = \left(\frac{3\pi(1-a^2)}{2\sqrt{2}h}\right)^{2/3}, \quad A = \frac{-2ah}{\pi(1-a^2)}. \tag{39}$$

The single-vortex self-similar solution for the flow is given by Eqs. (28) and (30) with $n = \frac{2}{3}$ and $\Lambda = \frac{3}{5}$.

For the vortex-sheet method, the single-point-vortex solution determines the initial position of the core vortex and its initial strength. In the following we take $h = 1$ so that $a = \sqrt{1/5}$, which corresponds to the case that the main pipe and the side branch have equal widths.

To start off the vortex-sheet method, five panels with a constant circulation $\Gamma(s) = \Gamma_v$ distribution are attached to the upstream edge along a streakline of the flow. The vortex sheet starts to increase in length and to wind around the point vortex. During the calculation the angular extent of the vortex sheet is limited to a maximum angle θ_v. The adaptive re-panelling scheme is used during the calculation.

The time step is determined by allowing a maximum displacement of a fraction $\tilde{\sigma}$ of each individual panel width. In addition the derivative of the transformation function is not allowed to vary more than 20% on each individual panel.

Figure 10 presents the computed results of the impulsively started flow in a T-junction for $0 < tU_0/H < 3.5$. During this period the vortex sheet grows continuously and reaches the downstream edge. The parameters used for the computation are given in Table II. When the vortex sheet hits the downstream edge the vortex sheet splits into two parts; one convects into the side branch, the other convects into the main pipe. For $tU_0/H = 1.5$ and $tU_0/H = 2.5$ the characteristics of the solution are shown in Fig. 11. At $tU_0/H = 1.5$, the vortex distribution is quite regular, with a local maximum value of the vortex distribution corresponding with a local maximum of the curvature of the sheet. This point is indicated by (1) in Fig. 11. Furthermore, again the vortex sheet leaves the upstream edge tangentially, while the curvature at the edge is infinite, similar to the case of a separated flow around an infinite 90°-wedge. At $tU_0/H = 2.5$, when the vortex sheet nearly hits the downstream edge, the vortex distribution has a peak value at the point of the sheet closest to the downstream edge, while also the curvature has a maximum value at that point (indicated by (1) in Fig. 11). At $tU_0/H = 3.5$, due to the Kelvin–Helmholtz instability of the straight vortex sheet, vorticity starts to concentrate into rolled-up regions. The wavenumber of this instability is determined by the chosen value of the parameter Δs_{max} of the numerical scheme [13, 19].

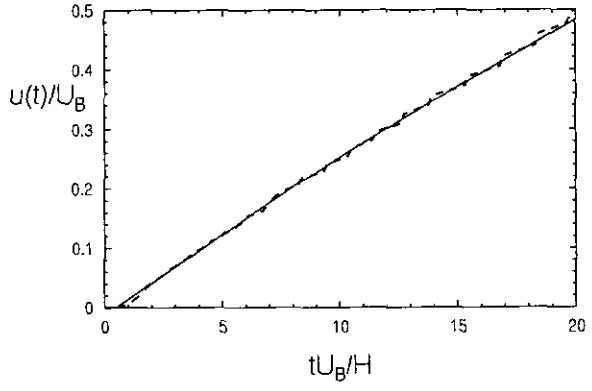

FIG. 12. Main flow velocity in the T-junction: (– – – –) velocity corresponding to maximum pressure difference $\Delta p = 50$ Pa (———) least squares fifth-degree polynomial fit.

3.3. Experiment

3.3.1. Flow Visualization

To verify the numerical results of the convection and the roll-up of the vortex sheet an experimental setup has been built to visualize the starting flow in a T-junction. The T-junction consists of square brass pipes of 3.0-cm width. The cavity has a depth of 6.0 cm, which is twice the side branch width. For visualization purposes, part of the side walls of the T-junction are glass windows.

A pressure difference over the system is obtained by decreasing the pressure in the laboratory with the help of the ventilation system of the building. The room in which the experiment has been carried out has a volume of 40 m^3,

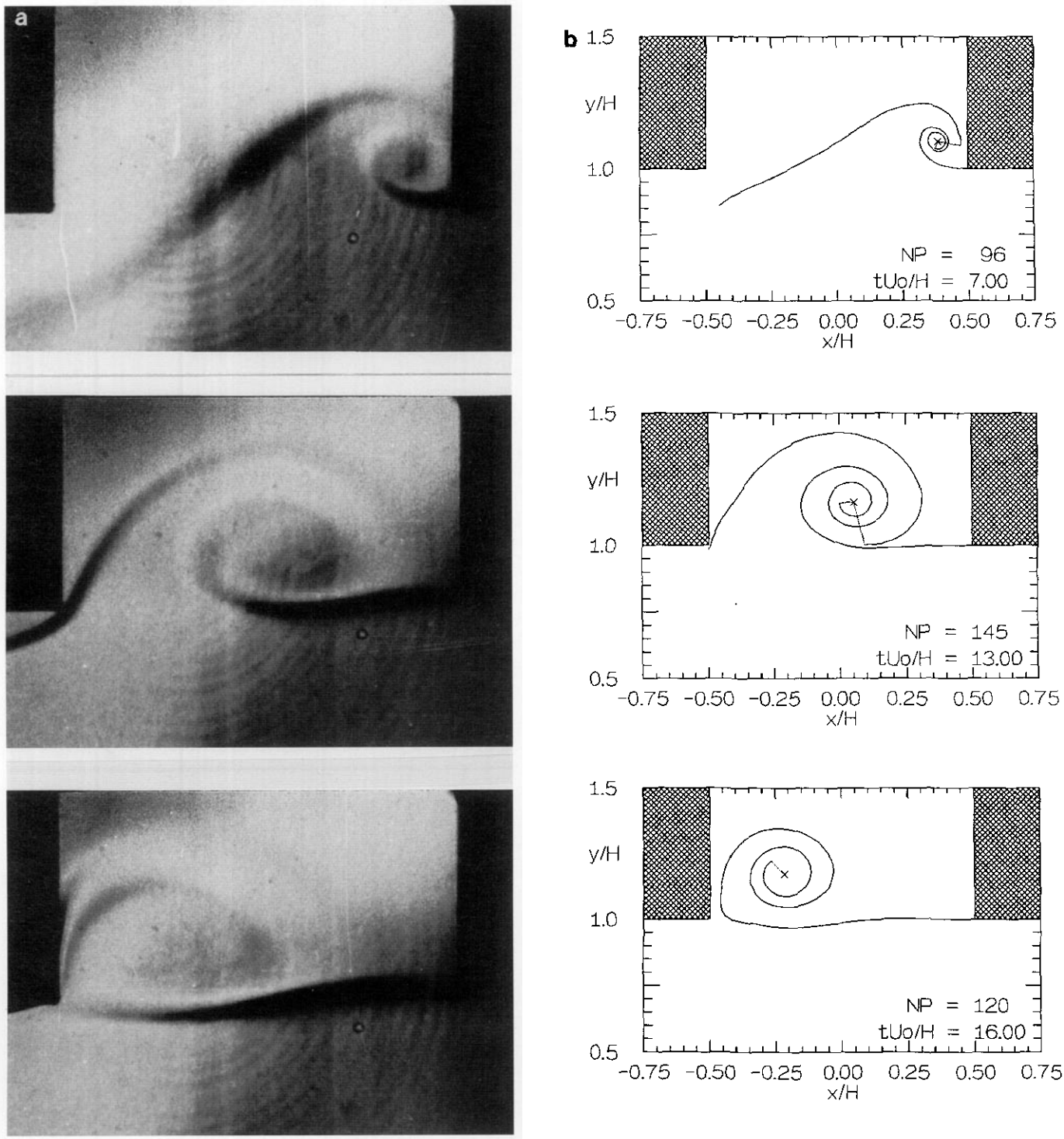

FIG. 13. Starting flow in a T-junction: (a) flow visualization at three moments of time; (b) results of a numerical simulation by the vortex-sheet method by using the measured velocity as a function of time at corresponding moments in time.

while the laboratory building which is used as a high-pressure supply has a volume of 3600 m^3. The pressure difference used for the present flow visualisation is 50 Pa. This pressure difference Δp is measured within 2-Pa accuracy by means of a Betz water manometer.

The high pressure room is connected to the main pipe by a contraction which yields a uniform velocity distribution in the upstream part of the main pipe. The operating pressure during the experiments was close to atmospheric pressure and the temperature close to room temperature (295 K). A standard schlieren method was used to visualize the flow. By injecting CO_2 in the side branch a refractive index variation is created across the shear layer enabling its visualization. Prior to each experiment the cavity was filled with CO_2. Therefore, in the schlieren pictures a contact line is observed between the gas originally inside the cavity and the air in the main pipe. The contact line contains no vorticity. A nanolite spark discharge provides a light pulse of about 80-na duration. In order to obtain a visualization at a well-defined point in time, the nanolite light source can be triggered by a hot wire anemometer, placed just upstream of the side branch. With the hot wire anemometer, the development in time of the main flow velocity is measured after opening the valve. The rise in the velocity with time since the opening of the valve (within approximately 1 ms) is given in Fig. 12. The maximum attainable velocity is equal to the Bernoulli velocity; i.e., $U_{max} = \sqrt{2\Delta p/\rho_0}$, with Δp as the initial pressure difference across the valve.

Figure 13[a] shows results of the flow visualization of the starting flow in the T-junction for three moments in time for $\Delta p = 50$ Pa. Separation of the flow at the upstream edge causes the formation of a vortex layer. Right at the beginning of the motion, the vortex layer rolls up and the shear layer with its vortical structure convects with the local flow velocity in the direction of the downstream edge.

Upon reaching the opposite edge, part of the vortex layer is forced into the side branch. Under influence of a Kelvin–Helmholtz-like instability the not yet rolled-up part of the vortex sheet in the T-junction starts to distort and, at times later than shown in Fig. 13, rolls up into secondary vortices. The instability of the vortex layer is more pronounced when the experiment is performed at a higher pressure difference than 50 Pa which results in an increased strength of the shear layer of smaller thickness (shorter times) [19].

Using a fifth-degree fit of the measured velocity rise (see Fig. 12), a calculation has been performed with the vortex-sheet method. In the numerical simulation, passive tracer particles have been introduced which initially are located at the intersection of the main pipe and the side branch. The tracer particles move with the local flow velocity and correspond directly to the contact line visible in the flow visualisation (see Fig. 13).

The results of the vortex-sheet method at moments in time corresponding to the time of visualisation are presented in Fig. 13[b]. The solution obtained with the vortex-sheet method is in fair agreement with the results of the flow visualization. Differences are probably due to the relatively low value of the Reynolds number in the experiment Re $\approx$ 2000.

4. CONCLUSIONS

The second-order vortex sheet method proposed by Hoeijmakers and Vaatstra [12] has been extended to describe the generation of vorticity at sharp edges. This has been accomplished by introducing the Kutta condition at sharp edges and a conformal mapping of the flow to a half-plane. The latter facilitates the use of symmetry conditions to exactly satisfy the stream surface condition on solid surfaces. The method has been applied to simulate in the time domain the starting flow past a semi-infinite wedge and the impulsively started flow in a T-junction. For the first application, a comparison with the time-invariant self-similar solution obtained by Pullin [17] shows a good agreement between the self-similar solution and the present results for long times. Although the vortex sheet separates from the solid edge tangentially, the curvature of the vortex sheet tends to infinity at the sharp edge.

The second application of the method shows that the method is able to simulate the internal flow in a T-junction accurately, where the separating flow at the upstream edge also leaves the edge tangentially. When the vortex sheet collides with the downstream edge, a Kelvin–Helmholtz instability of the remaining part of the vortex sheet is triggered. A comparison of the results of the vortex-sheet method with flow visualisation of the starting flow in a T-junction shows a fair agreement.

ACKNOWLEDGMENTS

This project is part of the Ph.D. thesis by the first author which is supervised by Professor G. Vossers and Dr. A. Hirschberg and is financially supported by the Netherlands Foundation for Fundamental Research on Matter (FOM/STW) under project number ETN 71.1403 and the N. V. Nederlands Gasunie. The authors thank R. Bastiaans for his contribution to the numerical study and L. M. B. C. Schoenmakers for the visualisation of the flow in the T-junction.

REFERENCES

1. L. Rosenhead, *Proc. R. Soc. London A* **134,** 170 (1931).
2. H. Aref, *Annu. Rev. Fluid Mech.* **15,** 345 (1983).
3. A. J. Chorin and P. S. Bernard, *J. Comput. Phys.* **13,** 423 (1973).
4. R. Krasny, *J. Fluid Mech.* **184,** 123 (1987).
5. R. R. Clements and D. J. Maull, *Prog. Aeronaut. Sci.* **16**(2), 129 (1975).
6. P. G. Saffman and G. R. Baker, *Annu. Rev. Fluid Mech.* **11,** 95 (1979).
7. A. Leonard, *J. Comput. Phys.* **37,** 289 (1980).
8. H. W. M. Hoeijmakers, *AGARD CP* **342**(18), 1 (1983).
9. H. W. M. Hoeijmakers, *AGARD CP* **494**(1), 1 (1990).
10. T. Sarpkaya, *J. Fluids Eng.* **111,** 5 (1989).
11. M. Mokry and W. J. Rainbird, *J. Aircraft* **12**(9), 750 (1975).

12. H. W. M. Hoeijmakers and W. Vaatstra, *AIAA J.* **21**(4), 516 (1983).
13. H. W. M. Hoeijmakers, Ph.D. thesis, Delft University of Technology; published as National Aerospace Laboratory, Amsterdam, the Netherlands, NLR Report TR 88088 U, 1989.
14. P. T. Fink and W. K. Soh, *Proc. R. Soc. London A* **362,** 195 (1978).
15. L. N. Trefethen, *SIAM J. Sci. Stat. Comput.* **1**(1), 82 (1980).
16. R. R. Clements, *J. Fluid Mech.* **57**(2), 321 (1973).
17. D. I. Pullin, *J. Fluid Mech.* **88**(3), 401 (1978).
18. N. Rott, *J. Fluid Mech.* **1,** 110 (1954).
19. M. C. A. M. Peters, Ph.D. thesis, Eindhoven University of Technology, 1993, ISBN 90-386-0282-0.
20. C. E. Brown and W. H. Michael, *J. Aeronaut. Sci.* **21,** 690 (1954).
21. J. M. R. Graham, *I. C. Aero Report 77-06*, pp. 1–22, 1977 (unpublished).
22. G. J. Clapworthy and K. W. Mangler, *Royal Aircraft Establishment T. R. 74150*, pp. 1–44, 1974 (unpublished).